Tanzania Journal of Science 45(2): 279-296, 2019 ISSN 0856-1761, e-ISSN 2507-7961

Assessment of the Effect of Acid Activation of Kaolin from Malangali on Water Defluoridation

Hosea E Shuma[1], Lupituko L Mkayula[2], Yahya MM Makame[3]
Chemistry Department, University of Dar es Salaam,
P. O. Box 35061, Dar es Salaam, Tanzania.
Email addresses: shuma.hosi@yahoo.com (Shuma); lupitukollmkayula@gmail.com (Mkayula); yahya.makame@gmail.com (Makame)

Abstract

Malangali kaolin clay was activated by means of an acid for defluoridation studies. The Acid Activated Malangali Kaolin (AAMK) clay and the Untreated Malangali Kaolin (UMK) were both characterized using spectroscopic and adsorption techniques. BET analysis of AAMK and UMK showed that both clays have mesoporosity characteristics with surface areas ranging from 55 to 58 m^2/g. Spectroscopic studies showed that in both clays the major mineral forms are kaolinites and albites with high amounts of SiO_2 and Al_2O_3. AAMK and UMK are endowed with surface functional groups such as OH, Si–O–Si, and Al–O–Al all of which being suitable for adsorption and ion exchange processes. The SEM and TEM images of the clays showed that both internal and external morphologies are slightly modified by means of acid activation. Defluoridation studies carried out in both Artificially Fluoridated Water (AFW) and Natural Fluoridated Water (NFW) under optimized conditions of temperature and pH produced results for the AAMK clay that had a much better demonstrable percentage fluoride removal in AFW by 86.30% and in NFW by 84.68%. The improved defluoridation is associated with clay surface modification rather than the insignificant surface area changes. The Langmuir, Freundlich and Temkin isotherms were well correlated with R^2 values greater than 0.95 indicating the involvement of fluoride chemisorption during defluoridation. The quality of the AAMK clay defluoridated water met the permissible standard limits of acceptance of WHO, US-EPA and the Tanzania Bureau of standards (TBS) recommendations for drinking water. The use of AAMK clay based adsorbent which is sourced readily and cheaply, is therefore, considered a worthy undertaking, which must be followed by further studies in order to shed more light on the defluoridation mechanism.

Keywords: Kaolin clay, defluoridation, physico-chemical, UMK, AAMK, fluoride

Introduction

The fluoride ion is an omnipresent naturally occurring chemical species of rocks and water. High concentrations of this ion in well water are due to dissolution of fluoride containing minerals from the rock into the groundwater. Some water authorities add fluoride to drinking water to strengthen teeth, while others must treat their water to remove excess amounts of this ion. The World Health Organization (WHO 2004) established a guideline value of 1.5 mg/L for fluoride in drinking water based on a consumption of 2 litres of water per day, where it recommended that artificial fluoridation of water supplies should not exceed the optimal fluoride level of 1.0 mg/L (WHO 2004). The United States Environmental Protection Agency (US EPA 2009) has set the primary standard (enforceable limit) at 4 mg/L for fluoride in drinking water, although the secondary standard (non-enforceable) for US drinking water supplies is 2 mg/L (US EPA 2009). In Tanzania, the limit for fluoride concentration in drinking (potable) water is 1.5–4 mg/L and the limit for bottled/packed water is 1.5 mg/L

(TBS 2008a, TBS 2008b). Excess fluoride in water leads to fluorosis effects from mild dental to crippling skeletal fluorosis as the level and period of exposure increase.

Crippling skeletal fluorosis is a major cause of morbidity in some regions of the world (Fawell et al. 2006). Incidences of fluorosis associated with excess fluoride in groundwater have been reported from different countries including Tanzania, South Africa, Kenya, India, Sri Lanka, Turkey, Ethiopia, China, Ghana and Sudan. Tanzania is very severely affected with fluoride (Tomar and Kumar 2013) as it occupies some of the highly fluorotic East Africa rift valley areas, like Arusha, Kilimanjaro, Mwanza, Mara, Shinyanga and Singida regions. Other regions of Tanzania, like Tanga, Tabora, Kigoma and Dodoma are reported to be moderately affected (Thole 2013).

Searches for suitable materials and methods for water defluoridation are ongoing worldwide, and a variety of materials such as activated alumina (Srimurali and Karthikeyan 2008), activated carbon (Alagumuthu 2010) and other low-cost materials such as, kaolinite, bauxite, zeolite, bone char, calcite and fly-ash (Tikariha and Sahu 2013) have been investigated for their defluoridation efficacy. Most of these materials exhibited low fluoride adsorption capacity while some are very expensive (Gaikwad and Sasane 2013) or suffer from ethical rejection (Chakrabarty and Sarma 2012). Numerous researchers have studied physical and chemical properties of clay minerals in order to understand their adsorbing and catalytic properties (Kumar et al. 2013). It is therefore important to improve the low fluoride adsorption capacity through surface modification of the clay minerals. This may involve, chemical modification (ion exchange, acid or base treatment or binding with organic or inorganic anions) which alters the structure, surface functional groups and the specific surface area of clay and physical modification (thermal or microwave treatment) involves alteration of the mineral composition and crystalline structure of clay at elevated temperatures (Kumar et al. 2013).

Numerous studies have reported on the acid treatment of clays such as bentonite (Foletto et al. 2011), smectite or montmorillonite (Angaji et al. 2013), kaolin (Kumar et al. 2013, Gogoi and Baruah 2008), palygorskite-sepiolite (Barrios et al. 1995) and glauconite (Srasra and Trabalsi-Ayedi 2000). Different acid activated clay minerals may show different fluoride adsorption capacities since naturally occurring clays normally contain mixtures of clay minerals with varying compositions (Bjorvatn and Bårdsen 1997). Hydrochloric acid and sulfuric acid are the most widely used activation acids because they give superior results in specific surface areas, porosity and adsorption capacity (Ravichandran and Sivasankar 1997). Acid activated clays now find numerous applications in water defluoridation (Gogoi and Baruah 2008), catalysts in petroleum refining (Emam 2013), heavy metals removal (Bhattacharyya and Gupta 2008), and bleaching materials for vegetable and mineral oils (Aishat et al. 2015). In Tanzania, fluoride removal using Pugu kaolin clay of non-activated and thermally activated was 41% and 53.6% (Peter 2009). Also, fluoride removal using thermally activated bauxite (Usambara Mountains) and kaolinites (Pugu) showed soil rich in bauxite was better than kaolinites (Peter 2009) and percentage fluoride removal using non-activated and thermally activated Pugu kaolin clay were 41% and 53.6%, respectively (Peter 2009).

In this study, an investigation on water defluoridation using Malangali kaolin clay (AAMK and UMK) was undertaken for both natural and artificial fluoride rich–water. The physicochemical quality parameters of the defluoridated water were also assessed.

Materials and Methods

Materials and reagents

Kaolin clay was collected from Malangali in Iringa region, Tanzania. Analytical grade reagents, including sodium hydroxide,

hydrochloric acid, glacial acetic acid, sodium chloride, 1,2–cyclohexylenediaminetetraacetic acid and sodium fluoride, were purchased from Sigma Aldrich Company. The chemicals were used as purchased without further purification.

Preparation of Acid Activated Malangali Kaolin (AAMK) clay

Malangali kaolin clay was crushed into powder and washed several times with distilled water to remove any particles attached to its surface. The powder was dried in an oven at 100 °C for 2 hours. A mixture of 100 g of dried kaolin clay with 500 mL of 0.5 M HCl solution was refluxed for 4 hours under the atmospheric pressure in a flat-bottomed flask equipped with a reflux condenser. The ensuing suspension of the (AAMK) clay was cooled to room temperature, filtered, washed until free from chloride and then dried at 80 °C overnight. Several samples were prepared and stored in desiccators for characterization and defluoridation studies.

Characterization of UMK clay and the prepared AAMK clays

The XRD patterns were obtained with an XRD InXiTU diffractometer (model BTX 231) in the Geology Department, University of Dar es salaam (UDSM). Both AAMK and UMK clay were crushed and sieved to get a powder with particle size less than 100 µm. They were each packed into an aluminium holder, which was then placed in a goniometer and bombarded with X–rays generated from cobalt tubes.

XRF analysis was carried out using a Bruker XRF Spectrometer (Model S8 Tiger) at SEAMIC located in Kunduchi, Dar es Salaam. Powdered samples were compressed under a pressure of 200 kN to form circular pellets with a diameter of 34 mm. The pellets were placed in aluminium cups, which were later placed in the XRF spectrometer to garner from them information about the elemental and percentage composition of the sample clays.

Attenuated Total Reflection–Fourier Transform Infrared Spectroscopy (ATR–FTIR) analysis of clay samples was carried out using Alpha ATR–FTIR spectrometer (Model Bruker optic GmbH 2011) in the Chemistry Department, University of Dar es Salaam. The clay samples were ground to a fine powder and then each sample was pressed against a high refractive index prism to allow for the infrared light to be reflected internally in the prism thus producing the required wave numbers in the IR detector and internal morphology. The crystal structure and elemental compositions were analyzed by Scanning Electron Microscopy (SEM) incorporated with Zeiss Ultra plus FEG SEM and a Transmission Electron Microscopy–Energy Dispersive X–ray (TEM–EDX) incorporated with JEOL 1010 TEM coupled with energy dispersive X–ray spectrophotometer at the University of Zululand. The observations were stored and analyzed using a software imaging system called iTEM.

The surface area, pore size distribution and pore volume were determined from nitrogen adsorption–desorption isotherms obtained at 77.35 K using a Quantachrome instrument (model NOVA 1200e) in the Chemistry Department, University of Dar es Salaam. A sample of about 1 g was used for the adsorption measurements. Then, analyses were carried out using a NOVA Win software to calculate the BET surface area, pore volume, and pore size distributions in accordance with the BJH method.

Fluoride adsorption tests

A column adsorption study was performed using both (AFW) and (NFW). An amount of 2.210 g of sodium fluoride was weighed with an analytical balance to prepare a stock solution of 1000 mg/L. From the stock solution several fluoride concentrations were prepared and subsequently used in fluoride adsorption capacity and efficiency tests. The NFW was taken from Ngurudoto, Arusha and used as obtained from the source. The

concentration of fluoride was measured using a Mettler–Toledo Seven Go Pro portable pH/Ion meter connected with a double junction fluoride ion selective electrode that is available in the Chemistry Department, UDSM. The fluoride adsorption capacity and efficiency from the residual fluoride concentration were calculated by using equations (1) and (2), respectively. Adsorption capacity, which is the equilibrium amount of adsorbed fluoride per unit mass of adsorbent (q_e) is given by:

$$q_e = \frac{C_0 - C_t}{m} \times v \qquad (1)$$

and

$$\% \text{ Adsorption} = \frac{C_0 - C_t}{C_0} \times 100\% \qquad (2)$$

where: C_o = is the initial fluoride concentration in mg/L, C_t = residual fluoride concentration at time t in mg/L, m = mass of adsorbent in g and v = volume of the solution used in the batch in mL. The data obtained were used to test the adsorption isotherm equations (Langmuir, Freundlich and Temkin).

Physico-chemical assessment of quality of defluoridated water

The physico-chemical water parameters of selected defluoridated samples for this study were based on APHA (APHA 1999), WHO (WHO 2003) and NHMRC, NRMMC (NHMRC, NRMMC 2011) guidelines for portable water. The physico-chemical water parameters investigated after water defluoridation included: pH, electrical conductivity, aluminium, total hardness, chloride, sulphate and sodium.

Results and Discussion

Characterization of UMK and AAMK clays

X-Ray Diffraction (XRD) analysis

The mineralogical compositions of the AAMK and UMK clays were determined by XRD. The diffractograms of both AAMK and UMK clays showed structural changes that occurred in the clay material after the acid treatment (Figures 1A and 1B). The diffractogram of UMK clay (Figure 1A) revealed the presence of albite ($NaAlSi_3O_8$), kaolinite ($Al_2Si_2O_5(OH)_4$) and zeolite ($NaAlSi_2O_6–H_2O$) as the constituent minerals of the clay. The peaks at 14.19°, 23.66°, 25.66° and 32.60° correspond to kaolinite, peaks at 16.09° and 25.74° correspond to albite and peaks at 6.43° and 35.74° correspond to zeolite. On the other hand, the only prominent minerals found were kaolinite and albite. The diffractogram for AAMK clay (Figure 1B) revealed peaks at 14.25°, 28.34°, 29.77° and 32.53° corresponding to kaolinite and peaks at 6.49°, 16.02° and 25.75° correspond to albite while none was for zeolites. There was a shift of peaks and a decrease in peak intensities from those observed in the UMK clay to AAMK clay. This is probably due to the broken lamellar structure and the partial decomposition of the structure of clay on heating with acid (Gogoi and Baruah 2008, Peter 2009).

X-Ray Fluorescence (XRF) analysis

The chemical compositions of the UMK and AAMK clays were determined by X–Ray Fluorescence (XRF) Analysis. Table 1 presents the percentage by weight of the elements present in UMK and AAMK clays as obtained from XRF analysis.

There was a high percentage by weight of SiO_2 and Al_2O_3 in both UMK and AAMK clays due to the presence of kaolinite mineral (Talabi et al. 2012) as shown in Table 1. The SiO_2/Al_2O_3 ratios of 1.59 and 1.57 in UMK and AAMK clays, respectively, resemble to the SiO_2/Al_2O_3 ratio of 1.46 in Ikere kaolinite (Talabi et al. 2012). Fe_2O_3 was present in large proportion compared to other oxides in both samples (UMK and AAMK clays), K_2O, SO_3, TiO_2, MgO, CaO, P_2O_5, Na_2O and ZrO_2 were almost negligible.

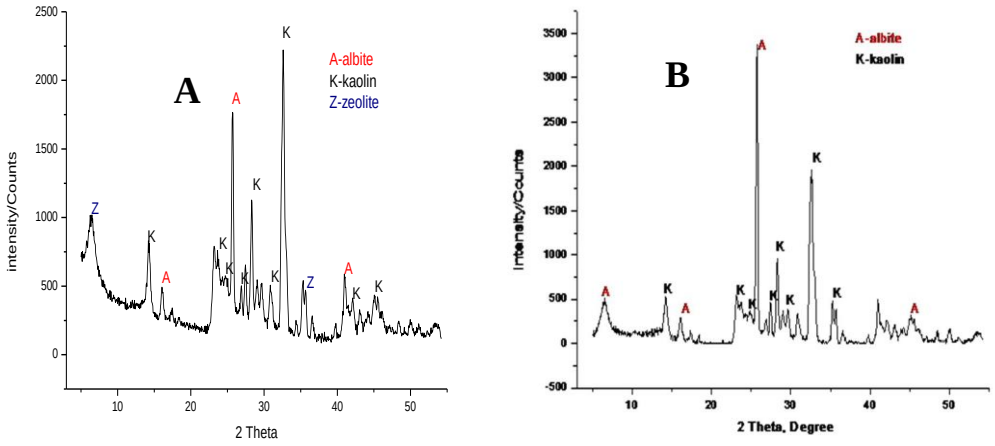

Figure 1: XRD patterns for UMK and AAMK Clay (A and B).

Table 1: Chemical composition in percentage (%) by weight of the UMK and AAMK clays

Component	Percentage Weight (%)		Component	Percentage Weight (%)	
	UMK	AAMK		UMK	AAMK
SiO_2	51.91	50.77	Cl	0.02	0.04
Al_2O_3	32.73	32.32	CaO	0.21	0.08
Fe_2O_3	1.69	1.73	P_2O_5	0.07	0.04
K_2O	0.14	0.13	Na_2O	2.59	1.95
SO_3	0.09	ND	ZrO_2	0.02	0.02
TiO_2	0.51	0.64	LOI	9.12	11.95
MgO	0.43	0.30			

ND = Not Detected

Attenuated Total Reflection-Fourier Transform Infrared Spectroscopy (ATR–FTIR) analysis

The functional groups of the AAMK and UMK clays were determined by ATR–FTIR analysis as shown in Figures 2A and 2B, respectively.

The ATR–FTIR spectra of UMK clay (Figure 2A) and AAMK clay (Figure 2B) samples revealed the effect of acid concentration on clay structure. The OH functional groups for both UMK and AAMK clays deduced from the stretching vibration bands observed respectively at 3690 and 3619 cm^{-1} correspond to the hydroxyl groups at the surface of the alumina octahedral layer that interact with the oxygen atoms of the adjacent silica tetrahedral layers. The absorption at this band in AAMK clay is slightly diminished with the treatment of acid; probably due to continued dehydroxylation (Kodama and Oinuma 1963). The shift of bands from 1113, 1025, 1000, 909 cm^{-1} in UMK to 1114, 1026, 1002, 910 cm^{-1},respectively, in AAMK clay. The 1114 and 1113 cm^{-1} is ascribed to asymmetric Si–O–Si stretching, 1025 and 1026 cm^{-1} is alternating Si–O–Si and Al–O–Al stretching vibrations and 1000, 1002 and 909 and 910 cm^{-1} is due to Al–OH vibrations. The intensity of –OH group bending vibrations at 1114.06 and 910.10 $cm^{-1}$and Al–OH decrease with increasing acid concentration due to the to the leaching of substituted Mg and Fe cations with increasing

acid concentration (Emmerich et al. 1999). In UMK clay, 787–416 cm^{-1} has the same intensity features as observed in AAMK clay (Angaji et al. 2013). Dissolution of tetrahedral silica from the clay structure is not likely to occur with lower acid concentration because the tetrahedral layer is relatively stable and is only affected at higher acid concentration while the octahedral aluminium layer is affected at lower acid concentration (Angaji et al. 2013).

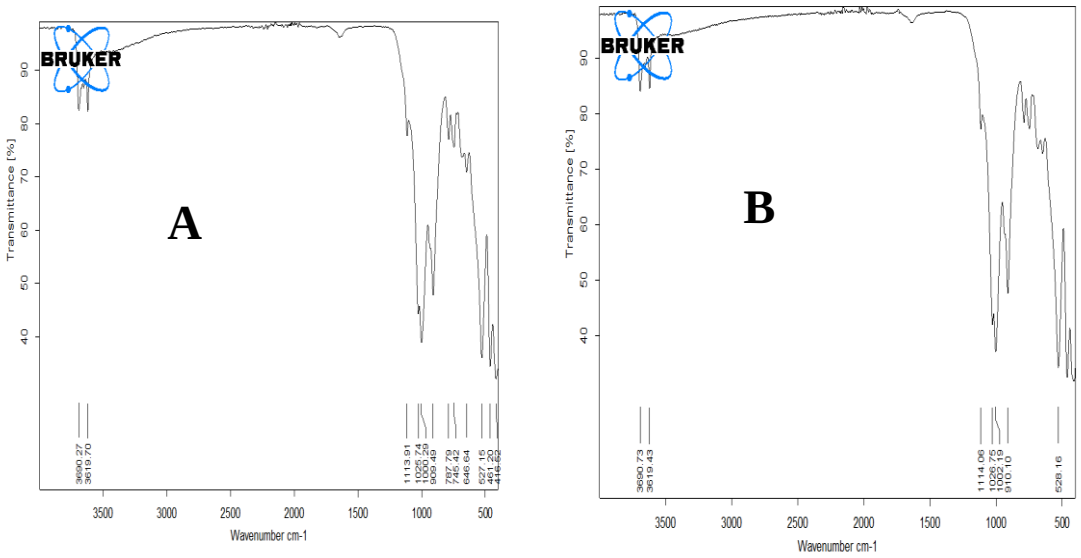

Figure 2: ATR-FTIR spectra for UMK and AAMK clays (A and B).

Scanning Electron Microscopy (SEM) Analysis

SEM imaging (Figures 3A and 3B) was done to analyze the surface morphology of UMK and AAMK clay. SEM images of UMK clay (Figure 3A) show the recognizable crystal faces that expose their angled edges on the surfaces of the clay. Figure 3B showed clearly the effect of acid treatment when the clay samples were treated with acid. There was crystal growth at the edges of the kaolinite sheets (Angaji et al 2013, Belver et al. 2002). This acid opened the platelets and produced a more porous structure which caused an increase in surface area. The morphology of AAMK clay became crispy (Kumar et al. 2013, Angaji et al. 2013).

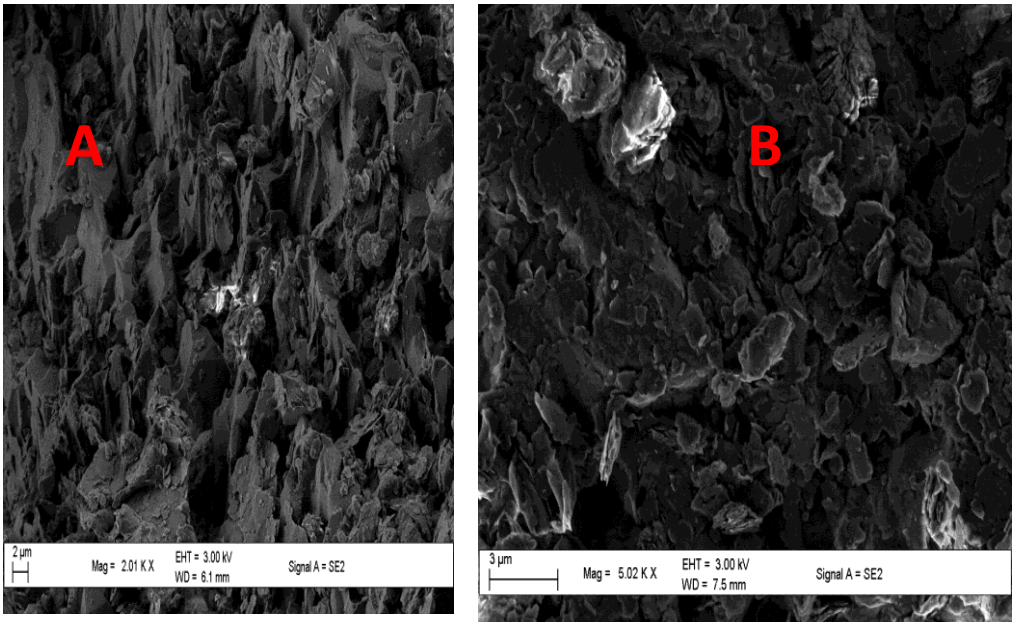

Figure 3: SEM images for UMK and AAMK clays (A and B).

Transmission Electron Microscopy–Energy Dispersive X–ray (TEM-EDX) analysis

TEM imaging was done to observe the internal morphology of UMK and AAMK clays. The TEM images (Figure 4A and 4B) show the presence of some pores in the internal structures of both UMK and AAMK clays. The EDX spectrums (Figure 4C and 4D) show that, both UMK and AAMK clays were composed of oxygen, silicon, aluminium, iron and zinc. The internal morphology of UMK and AAMK clays as viewed in the TEM images (Figures 4A and 4B) revealed that the morphology of the UMK clay was modified from the large clay layers of flat layers to smaller fragment pieces in AAMK clay (Angaji et al. 2013, Adjia et al 2013). The modification of the internal surface of the clay probably gives rise to the surface areas and pore volumes which depended on the concentration of acid added (Belver et al. 2002). The EDX spectrum (Figures 4C and 4D) shows the atomic percentage while the chemical compositions of UMK and AAMK clays are given in Table 2. The atomic percentage compositions of UMK clay (Figure 4C) were found to be 70.1%, 15.5% and 12.9% of oxygen, aluminium and silicon, respectively, and for AAMK clay (Figure 4D) were found to be 66.9%, 13.9% and 10.4% of oxygen, silicon and aluminium, respectively. The percentage compositions for AAMK clay are less than those for UMK clay. This is probably due to the leaching of the clay with inorganic acids that causes desegregation of the clay particles, elimination of mineral impurities and the dissolution of the internal layers, thus altering the chemical compositions and the structures of the clays (Belver et al. 2002, Senguptan et al. 2008). Also, the EDX spectrum confirmed that both UMK and AAMK clays contained kaolinite as major constituent of the clays due to high percentage of aluminium and silicon (Senguptan et al. 2008).

Nitrogen physisorption studies

Porosity characteristics of UMK and AAMK clays

The porosity characteristics of UMK and AAMK clays were investigated using the nitrogen adsorption–desorption technique. The surface areas were obtained using the BET method while the pore diameter and pore volumes were obtained using the BJH method. These values are given in Table 3.

Table 2: Summary of EDX results

Component	Relative weight (%)		Atomic (%)	
	UMK	AAMK	UMK	AAMK
Oxygen, O	57.02	47.59	70.1	66.9
Silicon, Si	22.20	17.32	15.5	13.9
Aluminium, Al	17.73	12.42	12.9	10.4
Sodium, Na	0.83	ND	0.7	ND
Iron, Fe	2.21	17.54	0.8	7.1
Zinc, Zn	ND	5.14	ND	1.8
Total	100	100	100	100

ND = Not detected

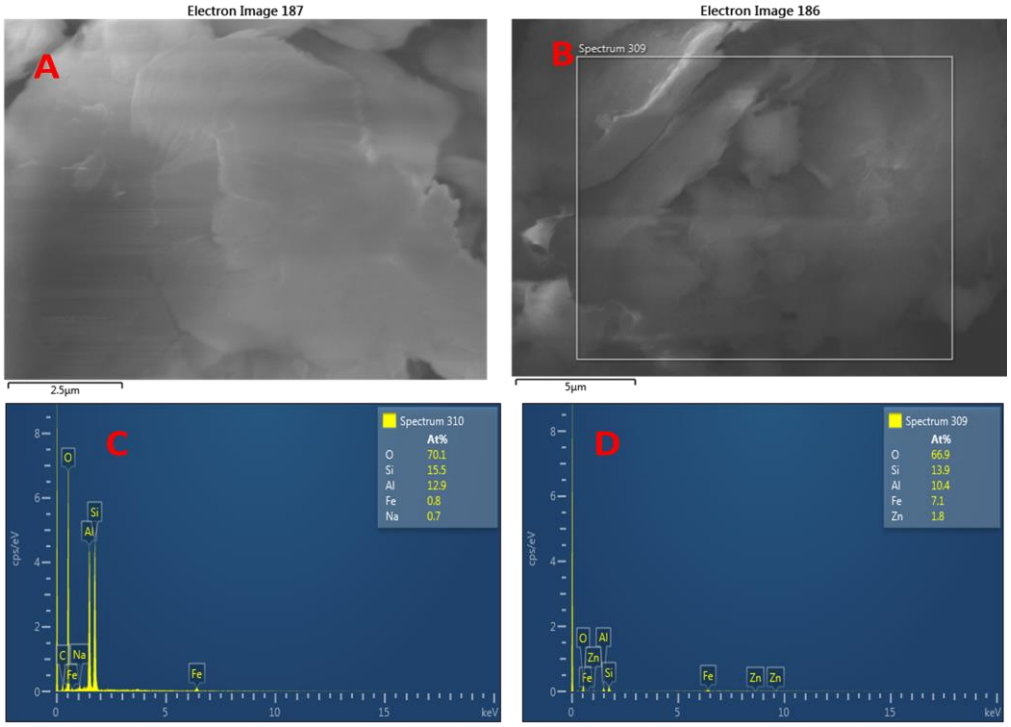

Figure 4: TEM images for UMK and AAMK clays (A and B) as well as EDX spectrum for UMK and AAMK clays (C and D).

Table 3: Porosity characteristics of UMK and AAMK clays

Sample ID:	Pore diameter (nm)	BET surface area (m^2/g)	Pore volume (cc/g)
UMK clay	3.7922	57.853	0.0104
AAMK clay	3.60	54.713	0.094

Nitrogen adsorption–desorption isotherms

The nitrogen adsorption–desorption isotherms obtained at 77.35 K for the UMK and AAMK clays are shown in Figures 5A and 5B, respectively. The BET surface area obtained using the nitrogen gas adsorption technique at 77 K (Table 3) decreased slightly from 57.853 m^2/g for UMK clay to 54.713 m^2/g for AAMK clay. This is probably due to refluxing of AAMK clay at high temperature that causes the adsorbent layers to collapse (Alymore et al. 1970). The pores diameter decreased from 3.7922 nm for UMK clay to 3.60 nm for AAMK clay which is a typical pore size characteristic for mesoporous materials ranging from 2 to 50 nm (Codon 2006). The pores volumes increased from 0.0104 cc/g of UMK clay to 0.094 cc/g of AAMK clay. This could be due to the leaching of kaolin through the removal of different cations from the surface or interlamellar space, and the subsequent formation of surface pores and cracks as well as the decrease in mineral sizes (Kumar et al. 2013).

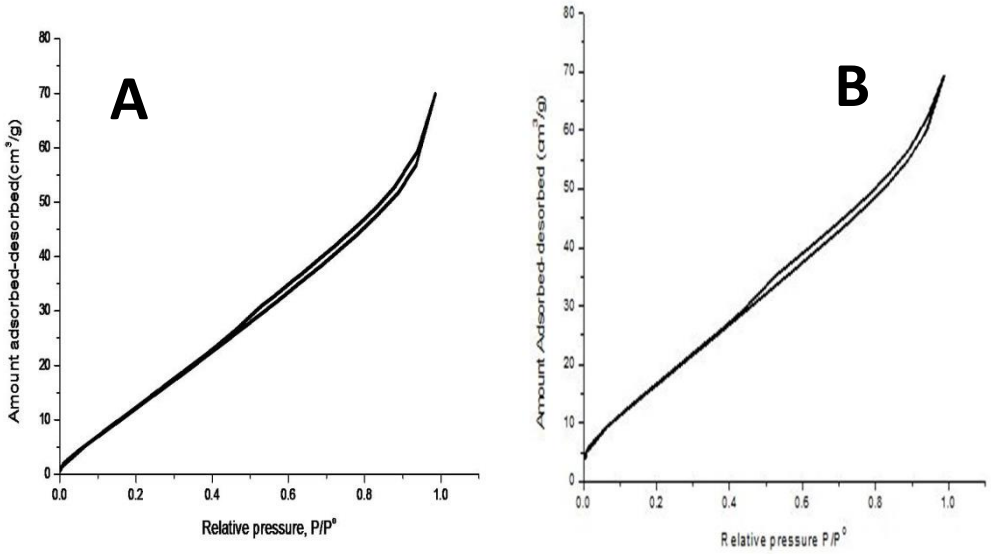

Figure 5: The nitrogen adsorption desorption isotherms for UMK and AAMK clay (A and B).

The shape of the nitrogen adsorption–desorption isotherms (Figures 5A and 5B) at 77 K was not changed by the acid treatment. Type IV isotherm which is a typical of mesoporous materials (Adjia et al. 2013, Olambo et al. 2016). The isotherms of UMK and AAMK clays also showed the presence of the hysteresis loop of type H3 at P/P^o greater than 0.4. This occurs due mesopore emptying associated with liquid nitrogen evaporating from the capillaries in mesoporous material (Strorck et al. 1998).

Optimization of parameters for water defluoridation using AAMK clay

The AAMK treated with 0.5 M HCl was preferred as an adsorbent for water defluoridation and was examined for its

efficiency in the adsorption of fluoride ions. Effects of various parameters were studied.

The effect of adsorbent dose

The experimental results (Figure 6) show that, AAMK clay adsorption capacity increases with the increase of adsorbent dosage. The optimum dose of adsorbent was found to be 5 g for fluoride concentration of 7.31 mg/L AFW and 6.393 mg/L NFW, which gave 79.21% and 81.96% fluoride ion removal efficiency, respectively. This was required to bring down the fluoride level between 1–1.5 mg/L as per WHO guidelines and 1.5–4 mg/L as per TBS and US–EPA guidelines. Figure 6 shows that the fluoride ion adsorption capacity of AAMK clay increases with addition of adsorbent dosage for both AFW and NFW. The electrolyte pair shows identical adsorption trends of adsorption capacity peaks when the adsorbent dosage of 15 g AAMK clay is reached. No further significant defluoridation capacity is observed due to the lack of fluoride ion in the water.

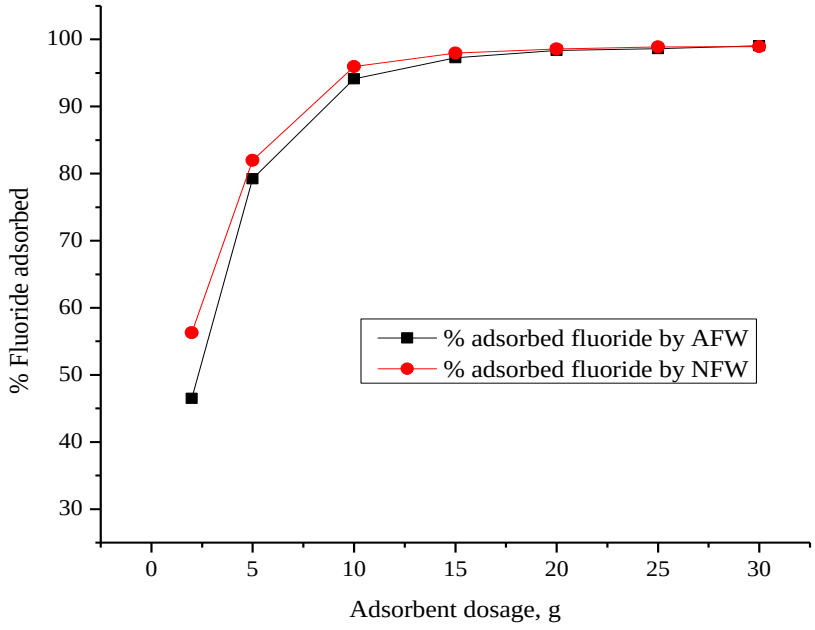

Figure 6: Effect of adsorbent dosage (conditions: room temperature, initial fluoride concentration = 7.31 mg/L AFW and 6.93 mg/L NFW, contact time = 30 min).

The effect of initial concentration

Figure 7 shows the effect of initial concentration of AFW for 5 g of AAMK clay ranging from 5 to 50 mg/L. While for NFW initial concentration was 6.59 and 11.35 mg/L and percentage adsorbed fluoride was found to be 84.68 % and 63.26 %, respectively. The adsorptive capacity of fluoride depends on the extent of Al-OH surfaces exposed to the surface of adsorbent which gets exhausted slowly with an increase of the initial fluoride concentration (Samson 1952). The optimum fluoride adsorption percent was 86.30% by using AFW.

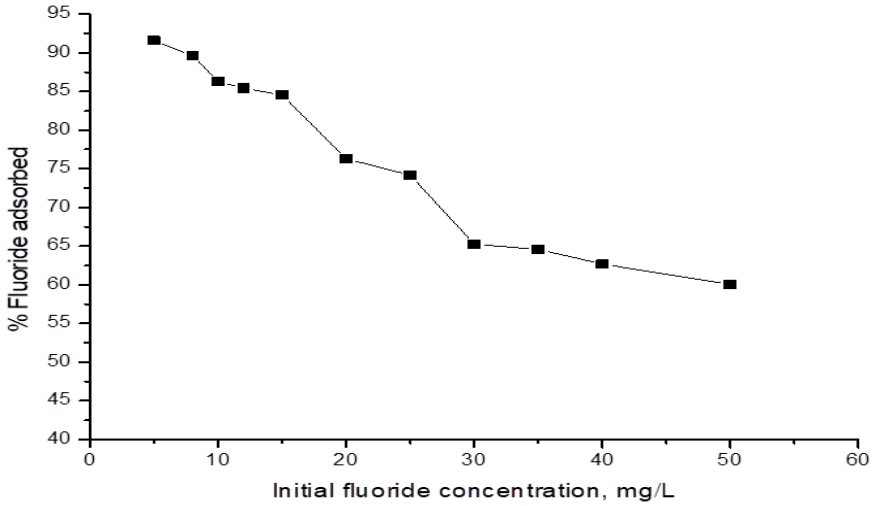

Figure 7: Effect of initial concentration for AFW (conditions: room temperature, contact time = 30 min and adsorbent dose = 5 g AAMK clay).

The effect of contact time

The experimental results (Figure 8) show that, generally, the percentage of adsorption of F^- was increasing with increasing contact time which reached a maximum after around one hour indicative of the attainment of the equilibrium point for the adsorption process. Specifically, the percentage removal of fluoride ions by both AFW and NFW was increasing with increasing contact time but followed separate paths towards the equilibrium point. This shows that access to binding sites on the 5 g AAMK clay was less competitive adsorption for AFW than for NFW. The NFW solution being natural is likely to have had unidentified ions that could have occupied the active sites in competition with F^- ions. The adsorption rate above about 15 minutes gets increasingly slow in both AFW and NFW due to lesser active sites (Srimurali and Karthikeyan 2008).

The effect of pH

For the adsorbent dose of 5 g AAMK clay, in the pH ranging from 5.0 to 9.0 the adsorption percentage was higher at lower pH (acidic media) and lower at higher pH (basic media). At pH ranging from 5.0 to 7.5 in AFW and from 5.0 to 6.5 in NFW (Figure 9) there was a significant change in fluoride ion percentage removal with maximum percentage removal of 93.12% at pH 7.5 for AFW and 91.87% at pH 6.5 for NFW. The adsorption of fluoride ions is increased due to availability of H^+ ions on the surface of the adsorbents, thus increasing surface sites for adsorption of fluoride ions (Fan et al. 2003). However, the decrease in defluoridation with increase in the pH is due to the fact that, at high pH values above 7, there is an abundance of negatively charged ions (OH^-) on the surface of the clay which hinder the adsorption of fluoride ions due to the electrostatic repulsion between negatively charged sites of the adsorbent and the fluoride ions, thus, the observed decline in the adsorption percentage (Fan et al. 2003).

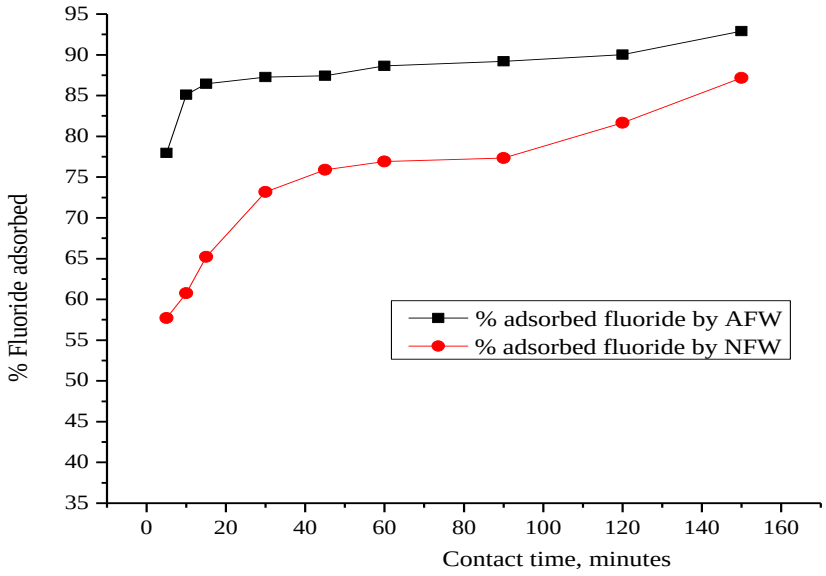

Figure 8: Effect of contact time (conditions: room temperature, adsorbent dose = 5 g of AAMK clay, initial fluoride concentration = 7.31 mg/L AFW and 6.93 mg/L NFW).

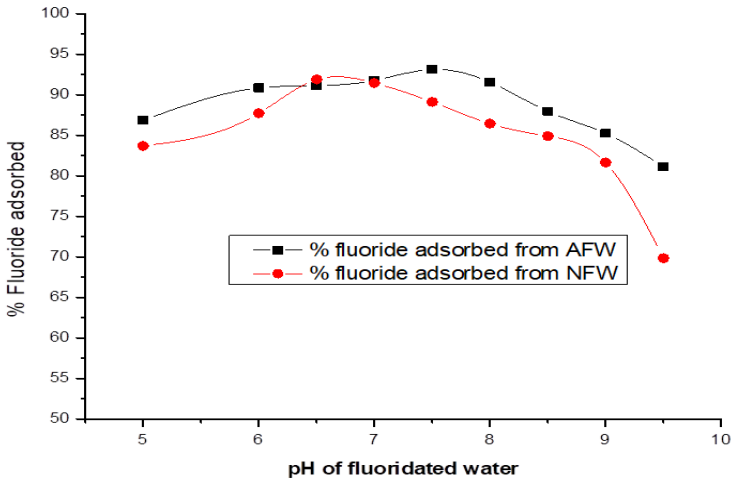

Figure 9: Effect of pH in fluoride ion adsorption (conditions: room temperature, initial fluoride concentration = 7.31 mg/L AFW and 6.93 mg/L NFW, contact time = 30 min, adsorbent dose = 5 g of AAMK clay).

The adsorption isotherms on AAMK clay

The Langmuir, Freundlich and Temkin adsorption equations were used to describe the data derived from the adsorption of fluoride ions from fluoridated water at concentrations ranging from 5 to 25 mg/L using AAMK. The

linear plots of Langmuir, Freundlich and Temkin equations are represented (Figures 10, 11 and 12). Table 4 contains a summary of important parameters from the Langmuir, Freundlich and Temkin isotherms. As presented in Figure 10 and Table 4, the Langmuir correlation coefficient, R^2 was found to be 0.976. The adsorption maximum, q_{max} was 0.13 mg/g; Langmuir constant, K_L value for AAMK was found to be 1.343 L/mg. In addition the Langmuir separation factor, R_L for initial fluoride concentration at a range of 5 to 25 mg/L was found to range from 0.130 to 0.028. Figure 11 and Table 4 presented the values obtained for a linear plot of log q_e against log C_e. The Freundlich correlation coefficient, R^2 was found to be 0.950. The Freundlich constants: K_F, $1/n$ and n were found to be 12.560, 0.468 and 2.137, respectively. Figure 12 and Table 4 show that the Temkin correlation coefficient, R^2 was 0.967, while the Temkin constants: A_T, B and b_T are 1.090 L/mg, 0.047 J/mol and 5.2714 x 10^4 J/mol, respectively.

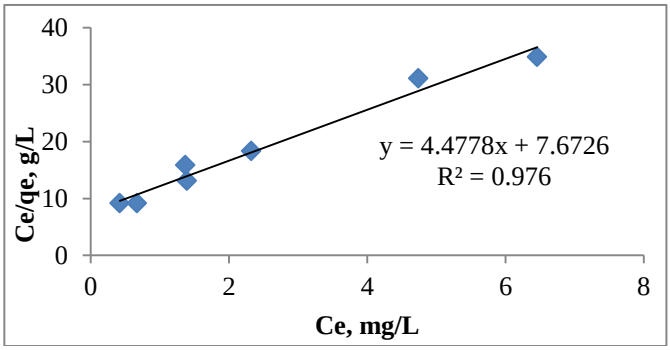

Figure 10: A linear Langmuir isotherm for AAMK.

Fluoride adsorption isotherm data have fitted well to the Langmuir isotherm, and the related correlation coefficient, R^2 was 0.976 (Figure 10). The high value of R^2 indicated that the uptake of fluoride ions occurred on the homogenous adsorption sites of AAMK by monolayer adsorption (Dada et al. 2012). The value of R_L for the initial fluoride concentration at a range of 5 to 25 mg/L was found to range from 0.130 to 0.028 for the Langmuir model. This indicates favourable sorption of fluoride ions onto the adsorbent (Olambo et al. 2016). The adsorption maximum, q_{max} was 0.13 mg/g, the Langmuir constant, K_L value of AAMK was found to be 1.343 L/mg.

From Figure 11, the Freundlich constants K_F and n were found to be 12.56 and 2.137, respectively. K_F, an intercept, the value of which indicates the adsorption capacity of the adsorbent, while the slope $\frac{1}{n}$ indicates the effect of concentration on the adsorption capacity and represents the adsorption intensity. The magnitude of K_F shows the ease of separation of fluoride ions from the aqueous solution and n indicates favourable adsorption. If the value of $n > 1$, this reflects a high affinity between adsorbate and adsorbent and it is indicative of chemisorption (Thambavani and Kavitha 2014). The value of R^2 (0.950) is indicative of a good Freundlich isotherm with a good fit.

The defluoridation data using AAMK clay also were fitted to Temkin isotherm (Figure 12). The results fitted well with correlation coefficient, R^2 of 0.967 with moderate adsorption, where A_T was 1.090 L/g (Vega et al. 2011). The heat of adsorption, b_T value was 5.2714 x 10^4 J/mol (52.71kJ/mol) which suggests a positive enthalpy of adsorption, ΔH_{ads}When the value ΔH_{ads} is between 40 and 800 kJ mol^{-1}, indicates that, defluoridation was due to the chemical interaction (i.e. chemisorptions) (Dada et al. 2012).

Therefore, the adsorption of fluoride ions on AAMK clay data were fitted into Langmuir, Freundlich and Temkin isotherms out of which the Langmuir adsorption model was found to have the highest regression value and hence the best fit.

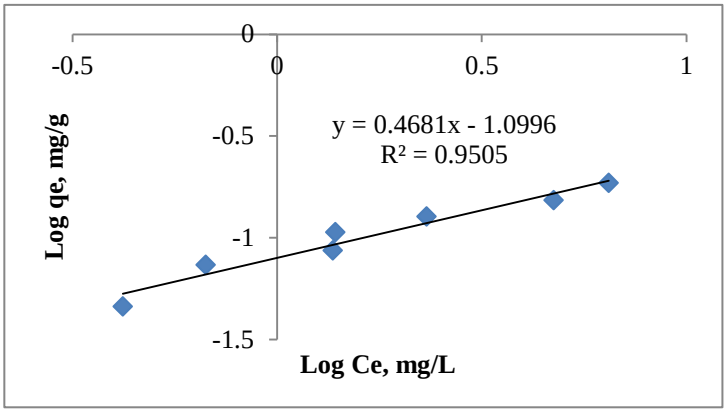

Figure 11: A linear Freundlich isotherm for AAMK clay.

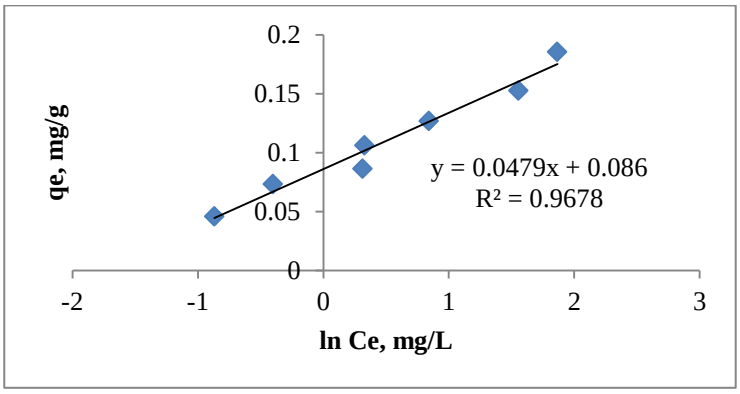

Figure 12: A linear Temkin isotherm for AAMK clay.

Table 4: Isotherm parameters obtained for Langmuir, Freundlich and Temkin isotherms

Isotherm model	Parameters	Results
Langmuir isotherm	R^2	0.976
	q_{max}	0.13 mg/g
	K_L	1.343 L/mg
	R_{eq}	0.130 – 0.028
Freundlich isotherm	R^2	0.950
	K_F	12.560 L/g
	$1/n$	0.468
	n	2.137
Temkin isotherms	R^2	0.967
	A_T	1.090 L/mg
	B	0.047
	b_T	5.2714 x 10^4 J/mol

Physico-chemical quality of defluoridated water

The levels of the physico-chemical water parameters of selected defluoridated samples investigated (pH, electrical conductivity, aluminium, total hardness, chloride, sulphate and sodium) are presented in Table 5.

Table 5: Results of some physico-chemical water parameters before and after defluoridation

Sample ID	Sodium (mg/L)	Aluminium (mg/L)	pH	Electrical conductivity µmhos/cm	Total hardness (mg/L)	Chloride (mg/L)	Sulphate (mg/L)
NW before	68.9683	ND	8.32	271.0	9.931	88.64	9.15
DW 30 min after	29.8446	0.2868	7.51	116.4	26.6625	88.64	9.02
DW 60 min after	27.9469	0.6100	7.72	113.4	5.3210	88.64	9.15
DW 90 min after	27.6019	0.7996	7.61	113.6	1.7728	110.80	9.32
DW 5 g after	30.3843	0.5169	7.58	118.4	2.3278	88.64	9.87
DW 10 g after	28.4813	ND	7.58	126.1	3.3018	177.29	0.43
DW 20 g after	33.9754	ND	6.94	150.4	3.5215	110.80	0.48
STD F^- 8 mg/L before	09.3385	ND	6.62	40.1	10.0903	66.48	8.72
F^- 8 mg/L after	10.3255	2.2584	7.29	115.5	2.4538	88.64	7.98
F^- 12 mg/L after	11.8229	2.7324	5.65	121.3	1.9218	11.80	0.35

ND = Not detected; NW = Natural water; DW = Defluoridated water

Water pH

The pH values (Table 5) of the selected samples ranged from 5.65 to 8.32. Most of the samples showed to be alkaline in nature and the ranges were within the permissible limit of 6.50–9.20 as prescribed by TBS and WHO for drinking water (TBS 2008b, WHO 2003).

Electrical conductivity

The electrical conductivity for water samples ranged from 40.1 to 271.0 µS/cm (Table 5). All the values were within the recommended limits of 8–10000 µS/cm set by WHO for drinking water.

Aluminium

The aluminium contents of water samples after treatments ranged from 0 mg/L to 2.73 mg/L (Table 5). Most of the aluminium contents were below the permissible limit of portable water. The values for aluminium contents should be below 2 mg/L according to TBS, 0.05 to a 0.2 mg/L for US EPA (US EPA 2013) and 0.1 to a 0.2 mg/L as per WHO for potable water.

Total hardness

Total hardness as $CaCO_3$ ranged from 1.77 mg/L to 26.66 mg/L (Table 5). This range is below the permissible values according to TBS and WHO for potable water.

Chloride

Chloride concentrations ranged from 66.48 mg/L to a 177.29 mg/L (Table 5). All the samples were below the permissible limit of 200 mg/L by WHO and TBS for potable water.

Sulphate

The concentrations of sulphate ranged from 0.35 to 9.87 mg/L (Table 5). The values were below the tolerance range of sulphate 200–600 mg/L as prescribed by WHO and TBS, and therefore, it is incapable of causing bad smells (Ezeribe et al. 2012).

Sodium

The concentrations of sodium in samples were below 68.96 mg/L (Table 5) which were within the permissible range of 20–250 mg/L as per WHO guidelines. However, for sodium in drinking water is based on the taste threshold of sodium in water of 180 mg/L as above 180 mg/L water will taste salty (NHMRC, NRMMC 2011).

Conclusion

The acid activated Malangali kaolin (AAMK) clay was refluxed with a 0.5 M HCl for 4 hours then washed and dried at 80 °C in an oven overnight. The UMK and AAMK clays were characterized using different techniques including XRD, XRF, ATR-FTIR, SEM, TEM and nitrogen physisorption study. XRD diffractograms for both AAMK and UMK clays showed that the main component of the clay is the kaolinite mineral, $Al_2O_3.2SiO_2.2H_2O$. The chemical compositions of both UMK and AAMK clays were SiO_2, Al_2O_3, Fe_2O_3, K_2O, SO_3, TiO_2, MgO, CaO, P_2O_5, Na_2O and ZrO. The SiO_2/Al_2O_3 ratios were 1.59 and 1.57 for UMK and AAMK clays, respectively. The ATR-FTIR of both UMK and AAMK clays showed the needed surface defluoridational functional groups. SEM and TEM showed the changes that occurred after treating the clay with acid. Nitrogen physisorption studies indicated that both UMK and AAMK clays were mesoporous materials with type IV isotherms and hysteresis loops of type H3. The defluoridation studies indicated that the AAMK clay is an effective adsorbent for adsorption of fluoride ions from both AFW and NFW with an optimum contact time for defluoridation of 15 minutes using 5 g of adsorbent. The AAMK clay could reduce the initial fluoride ions concentrations from 12 mg/L of AFW to 1.39 mg/L and 6.59 mg/L of NFW to 0.92 mg/L. The AAMK clay demonstrated to be an effective adsorbent at the room temperature and in the pH range of 6.5 to 9, which is the permissible range according to TBS and WHO for drinking water. The quality of defluoridated water was slightly affected by the chemical treatment of adsorbent; therefore the physicochemical concentrations of sodium, aluminium, pH, electrical conductivity, total hardness, chloride and sulphate were almost within the permissible limits according to WHO, US EPA and TBS. This work has demonstrated that the AAMK clay is an effective defluoridant in both AFW and NFW and this shows that the methods applied in the study are worthy following.

Acknowledgement

The authors would like to give their utmost thanks to the Chemistry Department at the University of Dar es salaam for providing the laboratory facilities. Many thanks also are due to the University of Zululand, South Africa, for analyses of the clay samples.

References

Adjia HZ, Villieras F, Kanga R and Thomas F 2013 Mineralogy and physico-chemical properties of alluvial clays from far North region of Cameroon: A tool for an environmental problem. *Int. J. Water Res. Environ. Eng*. 5: 54-66.

Aishat AB, Olalekan ST, Arinkoola AO and Omolola JM 2015 Effect of activation on clays and carbonaceous materials in vegetable oil bleaching. State of art review. *Br. J. Appl. Sci. Technol.* 5(2): 130-141.

Alagumuthu G, Veeraputhiran V and Venkataraman R 2010 Adsorption isotherms on fluoride removal: batch techniques. *Arch. Appl. Sci. Res.* 2(4): 170-185.

Alymore LAG, Sills ID and Quirk JP 1970 Surface area of homoionic illite and montmorillonite clay minerals as measured by the sorption of nitrogen and carbon dioxide. *Clays Clay Miner.*18: 91-96.

American Public Health Association (APHA) 1999 Standard methods for the examination of water and waste water. Washington DC.

Angaji MT, Zinali AZ and Qazvini NT 2013 Study of physical, chemical and morphological alterations of smectite clay upon activation and functionalization via the acid treatment. *World J. Nano Sci. Eng.* 3: 161-168.

Barrios MS, González LF, Rodriguez MV and Pozas JM 1995 Acid activation of a palygorskite with hydrochloric acid: Development of physicochemical, textural and surface properties. *Appl. Clay Sci*. 10: 247-258.

Belver C, Bañares Muñoz, MA and Vicente MA 2002 Chemical activation of a kaolinite under acid and alkaline condition. *Chem. Mater.* 14: 2033-2043.

Bhattacharyya GK and Gupta SS 2008 Adsorption of few heavy metals on natural and modified kaolinite and montmorillonite: A review. *Adv. Colloidal Interface Sci.* 140: 114-131.

Bjorvatn K and Bårdsen A 1997 Use of activated clay for defluoridation of water. In *Proceedings of the First International Workshop on Fluorosis and Defluoridation of Water* (pp. 40-45). International Society for Fluoride Research.

Chakrabarty S and Sarma HP 2012 Defluoridation of contaminated drinking water using neem charcoal adsorbent: Kinetics and equilibrium studies. *Int. J. ChemTech. Res.* 4: 511-516.

Codon JB 2006 Surface area and porosity determinations by physisorption measurements and theory, 1st ed., Elsevier, Netherlands.

Dada AO, Olalekan AP, Olatunya AM and Dada O 2012 Langmuir, Freundlich, Temkai and Dubinin-Radushkevich isotherms studies of equilibrium sorption of Zn^{2+} unto phosiphoric acid modified rise husk. *IOSR J. Appl. Chem.* 3: 38-45.

Emam AE 2013 Clay as catalyst in petroleum refining industry. *ARPN J. Sci. Technol*. 3: 356-375.

Emmerich K, Madsen FT and Kahr G 1999 Dehydroxylation behavior of heat treated and stream treated homoionic cis-vacant montmorillonites. *Clays Clay Miner*. 47: 591-604.

Ezeribe AI, Oshieke KC and Jauro A 2012 Physico-chemical properties of well water samples from some villages in Nigeria with cases of stained and molted teeth. *Sci. World J.* 7: 1-3.

Fan X, Parker DJ and Smith MD 2003 Adsorption kinetic of fluoride on low cost material. *Water Res.* 37: 4929-4937.

Fawell J, Bailey K, Clinton J, Dahi E, Fewtrell L and Magara Y 2006 Fluoride in drinking water. WHO drinking water quality series, London.

Foletto EL, Colazzo GC, Volzone C and Porto LM 2011 Sunflower oil bleaching by adsorption onto acid-activated bentonite. *Brazialian J. Chem. Eng*. 28:169-174.

Gaikwad RW and Sasane VV 2013 Assessment of ground water quality in and around Lonar Lake and possible water treatment. *Int. J. Environ. Sci.* 3: 1263.

Gogoi PK and Baruah R 2008 Fluoride removal from water by adsorption on acid activated clay. *Indian J. Chem. Technol*. 15: 500-503.

Kodama H and Oinuma K 1963 Identification of kaolin minerals in the presence of chlorite by X-ray diffraction and infra-red absorption spectra. 12th National conference *Clays Clay Miner.* XI, Pergamon Press. 236-249.

Kumar S, Panda AK and Singh RK 2013 Preparation and characterization of acids and alkali treated kaolin clay. *Bull. Chem. React. Eng. Catal.* 8: 61-69.

NHMRC, NRMMC 2011 Australian drinking water guidelines paper 6 national water quality management strategy. National Health and Medical Research Council, National Resource Management Ministerial Council, Commonwealth of Australia, Canberra.

Olambo FL, Philip JYN and Mdoe JEG 2016 The potential of Minjingu phosphate rock for water defluoridation. *Inter. J. Sci. Tech. Soc*. 4: 1-6.

Peter HK 2009 Defluoridation of high fluoride water from natural water sources by using soils rich in bauxite and kaolinite. *J. Eng. Appl. Sci.* 4: 240-246.

Ravichandran J and Sivasankar B 1997 Properties and catalytic activity of acid modified montmorillonite and vermiculite. *Clays and Clay Miner.* 45: 854-858.

Samson HR 1952 Fluoride adsorption by clay minerals and hydrated alumina. *Clay Miner. Bull.* 1: 266-271.

Senguptan P, Saikia PC and Borthakur PC 2008 SEM–EDX characterization of an iron rich kaolinite clay. *J. Sci. Ind. Res.* 67: 812-818.

Srasra E and Trabelsi-Ayedi M 2000 Textural properties of acid activated glauconite. *Appl. Clay Sci.* 17: 71-84.

Srimurali M and Karthikeyan J 2008 Activated alumina, defluoridation of water and household application. Proceeding of the *12th International water technology conference*. Alexandria, Egypt. 153-165.

Strorck S, Bretinger H and Maier WF 1998 Characterization of micro- and mesoporous solids by physisorption methods and pore size analysis. *Appl. Catal. A:* 174: 137-146.

Talabi AO, Ademilua OL and Akinola OO 2012 Compositional features and industrial application of Ikere kaolinite Southwestern Nigeria. *Res. J. Eng. Appl. Sci.* 1: 327-333.

Thambavani DS and Kavitha B 2014 Removal of chromium (VI) ions by adsorption using riverbed sand from Tamilnadu – A kinetic study. *Int. J. Res.* 1: 718-742.

TBS 2008a Tanzania standard, TZS 574. 2008. Packed (Bottled) water specification, Tanzania Bureau of standards, Dar es Salaam.

TBS 2008b Tanzania standards, TZS 789. 2008. Drinking (Portable) water-specification, Tanzania Bureau of standards, Dar es Salaam.

Thole B 2013 Groundwater contamination with fluoride and potential fluoride removal technologies for East and Southern Africa. In: Ahmad I and Dar M.A (ed.) *Perspectives in Water Pollution*. InTech.

Tikariha A and Sahu O 2013 Low cost adsorbent for defluoridation of water. *Int. J. Environ. Monit. Anal.* 1(2): 65-70.

Tomar V and Kumar D 2013 A critical study on efficiency of different materials for fluoride removal from aqueous media. *Chem. Cent. J.* 7: 51-65.

US EPA 2009 National primary drinking water regulations and national secondary drinking water regulation. United State Environmental Protection Agency.

US EPA 2013 Secondary drinking water regulations: Guidance for nuisance chemicals. Washington DC.

Vega FA, Andrade ML and Covelo EF 2011 Applying Freundlich, Langmuir and Temkin models in Cu and Pb soil sorption experiments. *Spanish J. Soil Sci.* 1(1): 20-37.

World Health Organization 2003 pH in drinking water. Background document for development of WHO guidelines for drinking water quality. Geneva, Switzerland.

World Health Organization 2004 Guidelines for drinking water quality, 3rd edition, Volume 1, Recommendation. WHO, Geneva.